Progress in Biophysics and Molecular Biology 144 (2019) 51–60

Contents lists available at ScienceDirect

Progress in Biophysics and Molecular Biology

journal homepage: www.elsevier.com/locate/pbiomolbio

Agonistic and antagonistic roles of fibroblasts and cardiomyocytes on viscoelastic stiffening of engineered human myocardium

Susanne F. Schlick [a, b, 1], Florian Spreckelsen [b, c, d, 1], Malte Tiburcy [a, b], Lavanya M. Iyer [a, b], Tim Meyer [a, b], Laura C. Zelarayan [a, b], Stefan Luther [a, b, c, d], Ulrich Parlitz [b, c, d], Wolfram-Hubertus Zimmermann [a, b, *], Florian Rehfeldt [e, **]

[a] Institute of Pharmacology and Toxicology, University Medical Center Göttingen, 37075, Göttingen, Germany
[b] DZHK (German Center for Cardiovascular Research), partner site Göttingen, 37075, Göttingen, Germany
[c] University of Göttingen, Institute for Nonlinear Dynamics, 37077, Göttingen, Germany
[d] Max Planck Institute for Dynamics and Self-Organization, 37077, Göttingen, Germany
[e] University of Göttingen, 3rd Institute of Physics – Biophysics, 37077, Göttingen, Germany

ARTICLE INFO

Article history:
Received 17 July 2018
Received in revised form
2 November 2018
Accepted 27 November 2018
Available online 12 December 2018

Keywords:
Engineered heart muscle
Fibroblasts
Cardiomyocytes
Collagen
Rheology
Nonlinear mechanics

ABSTRACT

Cardiomyocyte and stroma cell cross-talk is essential for the formation of collagen-based engineered heart muscle, including engineered human myocardium (EHM). Fibroblasts are a main component of the myocardial stroma. We hypothesize that fibroblasts, by compacting the surrounding collagen network, support the self-organization of cardiomyocytes into a functional syncytium. With a focus on early self-organization processes in EHM, we studied the molecular and biophysical adaptations mediated by defined populations of fibroblasts and embryonic stem cell-derived cardiomyocytes in a collagen type I hydrogel. After a short phase of cell-independent collagen gelation (30 min), tissue compaction was progressively mediated by fibroblasts. Fibroblast-mediated tissue stiffening was attenuated in the presence of cardiomyocytes allowing for the assembly of stably contracting, force-generating EHM within 4 weeks. Comparative RNA-sequencing data corroborated that fibroblasts are particularly sensitive to the tissue compaction process, resulting in the fast activation of transcription profiles, supporting heart muscle development and extracellular matrix synthesis. Large amplitude oscillatory shear (LAOS) measurements revealed nonlinear strain stiffening at physiological strain amplitudes (>2%), which was reduced in the presence of cells. The nonlinear stress-strain response could be characterized by a mathematical model. Collectively, our study defines the interplay between fibroblasts and cardiomyocytes during human heart muscle self-organization *in vitro* and underscores the relevance of fibroblasts in the biological engineering of a cardiomyogenesis-supporting viscoelastic stroma. We anticipate that the established mathematical model will facilitate future attempts to optimize EHM for *in vitro* (disease modelling) and *in vivo* applications (heart repair).

1. Introduction

Engineered human myocardium (EHM) presents structural, functional, and molecular properties of *bona fide* postnatal heart muscle (Tiburcy et al., 2017). Its advanced degree of organotypic maturation is exemplified by an anisotropic sarcomere assembly with ultrastructural evidence for the formation of M-bands as well as physiological responses to preload (Frank-Starling mechanism), stimulation frequency (Bowditch phenomenon), and pharmacological stimuli such as catecholamines. For EHM assembly, cardiomyocytes and fibroblasts are embedded in a collagen type I hydrogel and cast into preformed molds of suitable geometries.

Abbreviations: Cardiomyocytes, (CMs); human foreskin fibroblasts, (Fibs); engineered human myocardium, (EHM); large amplitude oscillatory shear, (LAOS).

* Corresponding author. Institute of Pharmacology and Toxicology, University Medical Center Göttingen, 37075, Göttingen, Germany.
** Corresponding author. University of Göttingen, 3rd Institute of Physics – Biophysics, 37077, Göttingen, Germany.
E-mail addresses: w.zimmermann@med.uni-goettingen.de (W.-H. Zimmermann), rehfeldt@physik3.gwdg.de (F. Rehfeldt).

[1] equally contributing first authors.

https://doi.org/10.1016/j.pbiomolbio.2018.11.011

After the onset of spontaneous beating (within 72 h) EHM are subjected to mechanical loading to further enhance maturation (Tiburcy et al., 2017). Additional means to enhance tissue maturation include the use of electrical stimuli at (near-)physiological frequencies (Godier-Furnémont et al., 2015; Ronaldson-Bouchard et al., 2018).

The use of defined cardiomyocyte and fibroblast populations mixed at an optimized ratio in a collagen hydrogel environment and exposure to mechanical loading to facilitate auxotonic contractions are key for the heart muscle self-assembly process (Tiburcy et al., 2017). The pivotal role of the initially less appreciated non-cardiomyocyte stroma cells, and here in particular fibroblasts, has now clearly been recognized (Kensah et al., 2013; Naito et al., 2006; Soong et al., 2012; Zhang et al., 2013). Alternatively, endothelial cells (Weinberger et al., 2016) or so called tri-culture models comprising cardiomyocytes, smooth muscle cells, and endothelial cells (Gao et al., 2018) have been developed. In each of these assemblies it is likely that the non-myocyte component exhibits some fibroblast-like activity, for example by epithelial/endothelial-mesenchymal transformation (EMT/EndMT (Li et al., 2018)) or cellular impurities in the applied cell populations.

The specific mode(s) of action underlying fibroblast-supported heart muscle assembly remain elusive, but may include the synthesis of cardiomyogenic extracellular matrix, paracrine crosstalk, and biomechanical stimuli mediated via biophysical interactions with the extracellular matrix. Moreover, it is quite likely that these processes occur in a time-sensitive manner. In this context, the process of early tissue consolidation, which leads to a macroscopically visible collagen hydrogel compaction within 1 h after casting of the EHM reconstitution mixture, is least understood (Tiburcy et al., 2014); compromised early tissue compaction is indicative for poor outcome, i.e., a failure to form force-generating EHM (systolic force amplitude: >1 mN/mm^2) within a timeframe of two to four weeks (Tiburcy et al., 2017).

In this study, we sought to determine the factors governing collagen hydrogel consolidation with a particular focus on *in situ* mechanical quantification of early EHM compaction as well as the specific roles of fibroblasts and cardiomyocytes during this process. We used rheological measurements to define distinct phases of cell-independent collagen gelation and cell-dependent collagen compaction. Here, we defined fibroblasts as the main contributors to collagen matrix stiffening and cardiomyocytes as “cellular antagonists” of this process. Since most biopolymers and biological tissues exhibit a nonlinear viscoelastic behavior (Storm et al., 2005), we also performed large amplitude oscillatory shear (LAOS (Ewoldt et al., 2008)) measurements to determine the cellular impact on strain-stiffening of the consolidated tissue. Finally, we propose a mathematical model characterizing mechanical stress as a function of strain and strain rate, which we view as an important step for future numerical simulations of cell-matrix interactions during EHM formation.

2. Results

2.1. Engineered human myocardium input cell populations and development

Engineered human myocardium (EHM; Fig. 1A) was generated by casting defined mixtures of collagen type I, human embryonic stem cell-derived cardiomyocytes (CMs), and human foreskin fibroblasts (Fibs) in circular molds; reconstitution mixtures comprising CMs and Fibs at a 2:1 ratio were recently identified to optimally support EHM formation (Tiburcy et al., 2017). We controlled CM (alpha-actinin: 95 ± 2%; n = 3) and Fib (CD90: 94 ± 5%, n = 3) purity by flow cytometry (Fig. 1B). Purity and identity of the respective cell populations were further confirmed by transcriptome analyses, showing the anticipated cell type specific transcript signatures for the CM and Fib populations (Fig. 1C). After casting of the EHM-reconstitution mixture, EHM undergo a first phase of matrix consolidation resulting in macroscopically visible compaction after 60 min (Tiburcy et al., 2014) and an on-set of rhythmic contractions within 72 h in culture; subsequent mechanical loading to support auxotonic contractions results in advanced tissue maturation (Tiburcy et al., 2017). This process is paralleled by the development of an anisotropic and well-structured functional syncytium (Fig. 1D).

2.2. Fibroblasts drive collagen type I hydrogel compaction

In order to investigate the role of fibroblasts for EHM compaction, mechanical behavior and functional maturation, we generated collagen I hydrogels without cells, with either CMs or Fibs, or with both cell types (EHM). We quantified the compaction process after 24 h and 72 h. In the presence of fibroblasts, collagen type I hydrogels were significantly more compacted than in the presence of either CMs or no cells at all (Fig. 2A and B). The compaction process was completed at 24 h for collagen type I hydrogels without cells, with CMs and with CMs plus Fibs. Collagen type I hydrogels populated with Fibs continued to compact (Fig. 2A and B). After 4 weeks, tissues were strikingly different as to their macroscopic appearance with a failure to compact in cell- and fibroblast-free models (Fig. 2B). Tissue compaction could further be quantified by the measurement of tissue thickness (i.e., the distance between the inner and outer tissue boundaries in mm: Collagen only 5.1 ± 0.3; +CM 4.8 ± 0.2; +Fib 1.1 ± 0.06; +CM/+Fib 1.3 ± 0.3; n = 12/9/10/12; Fig. 2C). Staining with Sirius red confirmed that collagen fibers were compacted markedly in the fibroblasts containing tissue (Fig. 2D). Interestingly, we also noted some collagen fiber compaction in the CM only tissue, which could be supported by contaminating mesenchymal fibroblast-like cells (~5% according to flow cytometry; Fig. 1B). The consequences of the failure to compact for contractile outcome could be confirmed by isometric force measurements with minimal twitch amplitudes in CM-only tissue versus maximal twitch amplitudes in the CM + Fib containing EHM (force of contraction [FOC] in mN at maximally effective extracellular calcium [4 mM]: 0.2 ± 0.05 vs. 1.2 ± 0.2; *p < 0.05 by two-tailed unpaired Student's t-test; n = 4/group; Fig. 2E).

2.3. Mechanical properties of collagen network formation

After the basic characterization of EHM consolidation and function from the first day to up to 4 weeks, we focused on the mechanical characterization of the applied collagen type I without a cellular component. Therefore, we first measured the temporal evolution of the shear storage G' and shear loss modulus G'' of pure collagen at 1% strain and a physiological frequency of 1 Hz to simulate the repetitive strain collagen would be exposed to in the human heart. The obtained data indicated that collagen stiffening by gelation is a material inherent process, which appears quickly after pH-neutralization and is completed after 30 min (Fig. 3). Average G' and G'' plateaued at 26.5 ± 0.8 Pa and 4.1 ± 0.3 Pa, respectively.

2.4. Differential contribution of fibroblasts and cardiomyocytes to collagen network consolidation

Subsequent mechanical characterization of collagen type I hydrogels with and without cells (CMs and/or Fibs) confirmed the finding of a completion of the cell-independent collagen gelation

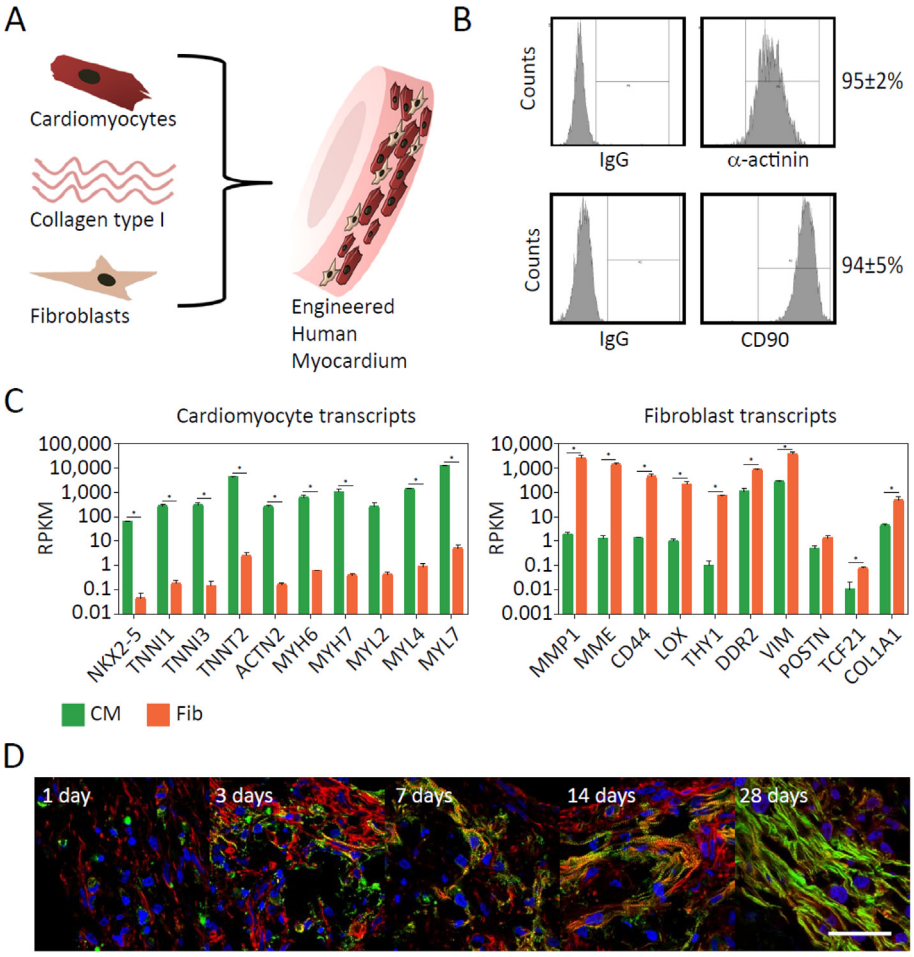

Fig. 1. Characterization of the engineered human myocardium (EHM) cell populations. (A) EHM were generated from human embryonic stem cell-derived cardiomyocytes (CMs) and human foreskin fibroblasts (Fibs) suspended in a collagen type I hydrogel (2:1 CM:Fib ratio). (B) Confirmation of input cell purity by flow cytometry for the CM marker "alpha-sarcomeric actinin" (ACTN2) and the Fib marker "CD90" (aka Thy-1). (C) Transcriptome analyses confirmed characteristic RNA profiles in CM and Fib populations (data n = 3/group); CM and Fib transcript signatures were recently reported in detail in Tiburcy et al. (2017); RPKM: Reads Per Kilobase Million. *P < 0.05 CM vs. Fib by unpaired, two-tailed Student t-test. (D) Whole-mount EHM immune fluorescence imaging at the indicated days after casting; sarcomeric actinin (green) labels CMs, f-actin (red), nuclei (blue); scale bar: 50 μm (all panels have the same magnification).

process within 30 min after pH-neutralization (Fig. 4A and B). Continuous collagen matrix stiffening was observed in collagen type I networks containing Fibs, with however a clear attenuation of the Fib-mediated stiffening process in the presence of CMs (resembling the EHM mixture). These findings were in line with the previously reported macroscopically visible compaction of EHM as early as 60 min after casting (Tiburcy et al., 2014) as well as the in this study documented continuous tissue compaction process (Fig. 2A–D). The associated changes in viscoelastic properties could be determined quantitatively by cone and plate shear rheology as changes of G′ and G″ as a function of time after the cell-independent collagen gelation was completed, i.e., 30–60 min after the start of the experiment (Fig. 4A–C). Collectively, these data identify distinct phases of cell-independent gelation (0–30 min) and largely Fib-dependent (in Fib and EHM samples) tissue compaction (>30 min), which appears to be modulated by cardiomyocytes in the EHM samples (Fig. 4D).

2.5. Differential Fib and CM transcriptomes during early EHM compaction

To interrogate potential molecular changes during fibroblast-dependent EHM compaction, we performed differential transcriptome analyses by RNA-sequencing. By comparing the cell transcriptomes at baseline, i.e., after a 30 min cell seeding and largely cell-independent collagen gelation phase without obvious differences in cell-induced viscoelastic properties, and after additional 60 min in which we observed either no further (in CM populated collagen) or Fib-mediated collagen hydrogel stiffening (Fig. 5A). As anticipated, a principle component analysis (PCA; Fig. 5B) of the RNA-sequencing data reflected for the most part (91% in principle component [PC] 1) the differences in cell composition: (1) CM: only cardiomyocytes; (2) Fib: only fibroblasts; (3) EHM: CM:Fib at a 2:1 input ratio. PC2 (7%) separated the single cell type hydrogel cultures from the mixed cultures comprising the same cells, suggesting a transcriptionally effective CM:Fib cross-talk. The transcriptional changes within the time-frame of 60 min of no (CM group) or Fib-mediated (Fib and EHM groups) collagen compaction were small as anticipated (Fig. 5B). It was however notable that Fibs in comparison to CMs presented a markedly enhanced differential transcription within the 60 min observation period (DEG; 1,379 vs. 369; Fig. 5C). From those, 202 DEGs were commonly regulated in all investigated groups and according to GO term analyses associated with "general tissue formation processes" (Supplemental Table 1). The Fib-specific expression profile (1,161 DEGs; Supplemental Table 1) included evidence for markedly enhanced transcriptional

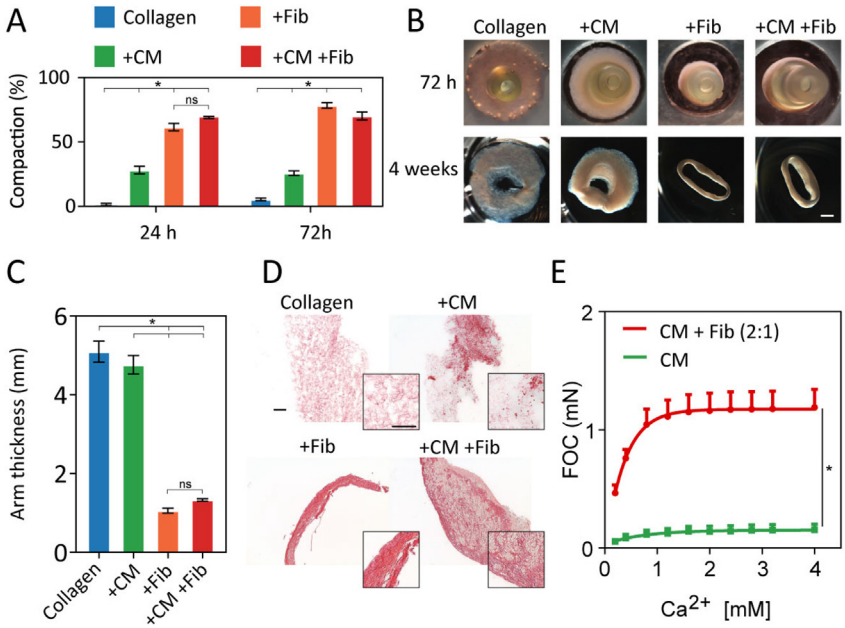

Fig. 2. Fibroblast controlled tissue compaction. (A) Collagen type I hydrogels were generated containing either no cells or Fibs (~430,000/tissue) and/or CMs (~860,000/tissue). Compaction was assessed 24 h and 72 h post-casting into circular PDMS molds with a central Teflon rod. *p < 0.05 vs. Collagen by 1-way ANOVA followed by Sidak multiple comparison test. (B) Representative images of compacted tissue at 72 h (within the casting molds) and 4 weeks of culture (free floating after release from the casting molds). Scale bar: 1 mm (applies to all panels). (C) EHM combined arm thickness at 4 weeks in culture; *p < 0.05 vs. Collagen or + CM as indicated by 1-way ANOVA followed by Tukey multiple comparison test, n = 9–12/group. (D) Sirius red tissue sections to highlight fibrillary collagen at 4 weeks in culture. Scale bars: 100 μm (overviews) and 400 μm (inset). (E) Force of contraction (FOC) of EHM (CM + Fib) and CM-only containing tissue after 4 weeks in culture; FOC was measured at 37 °C in Tyrode's solution under electric pulsed-field stimulation at 1.5 Hz; the characteristic increase in FOC as a function of increasing extracellular calcium is displayed. *p < 0.05 by 2-way ANOVA; n = 4/group.

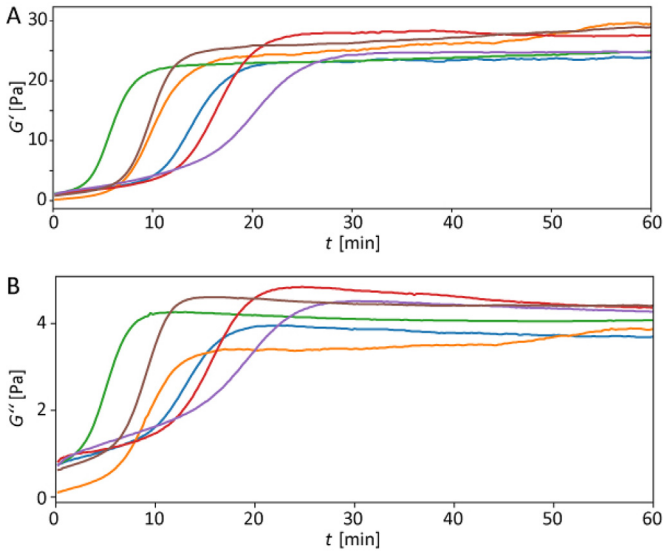

Fig. 3. Mechanical characterization of collagen type-I hydrogel gelation. Storage modulus G' (A) and loss modulus G'' (B) plotted as a function of time. Individual (n = 6) rheology measurements of cell-free collagen type I hydrogels were performed using a cone (2°) and plate bulk rheometer. Gelation of acidic acid solubilized collagen type I was started by pH-neutralization with NaOH at room temperature (23 °C).

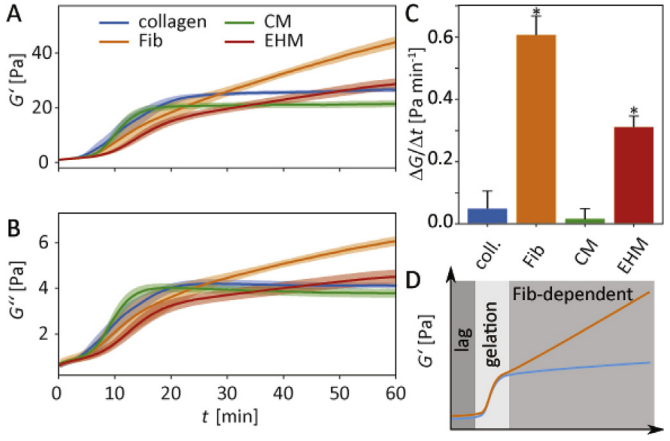

Fig. 4. Biophysical properties of consolidating cell-free and cell-containing collagen type I hydrogels. Samples of collagen type I containing no cells (Collagen; n = 6), CMs (n = 3), Fibs (n = 4), and both cell types (EHM; n = 4) were mechanically analyzed using a cone and plate rheometer. Applying fixed 1% strain at 1 Hz the storage modulus G' (A) and loss modulus G'' (B) were recorded over a timeframe of 60 min; extended measurements were technically difficult to perform due to the drying of the hydrogel formulation. (C) Average change of G′ as a function of time (ΔG'/Δt in Pa min^{-1}) during the 30–60 min (cell-dependent compaction) interval. *p < 0.001 vs. Collagen (coll.) by 1-way ANOVA and Tukey's multiple comparison. (D) Schematic summary describing the distinct phases of cell-independent collagen hydrogel gelation and Fib-dependent (in Fib and EHM groups) collagen hydrogel compaction.

activity and processes related to “heart development” and “extracellular matrix organization”, with for example an upregulation of SOX9, described as a master regulator of organ development and collagen expression (Hanley et al., 2008; Lacraz et al., 2017); this finding was in line with our earlier observation of a strong contribution of endogenously produced collagen type I in EHM formation (Tiburcy et al., 2011). The cardiomyocyte-specific 154 DEGs indicated enhanced endoplasmic reticulum (ER)-stress (Supplemental Table 1), which may trigger apoptotic processes. Interestingly, transcriptional signatures for the activation of “apoptotic processes” were markedly enhanced in the presence of Fibs and Fib-dependent matrix stiffening. This finding is in agreement with the observed over-proportional loss of cardiomyocytes

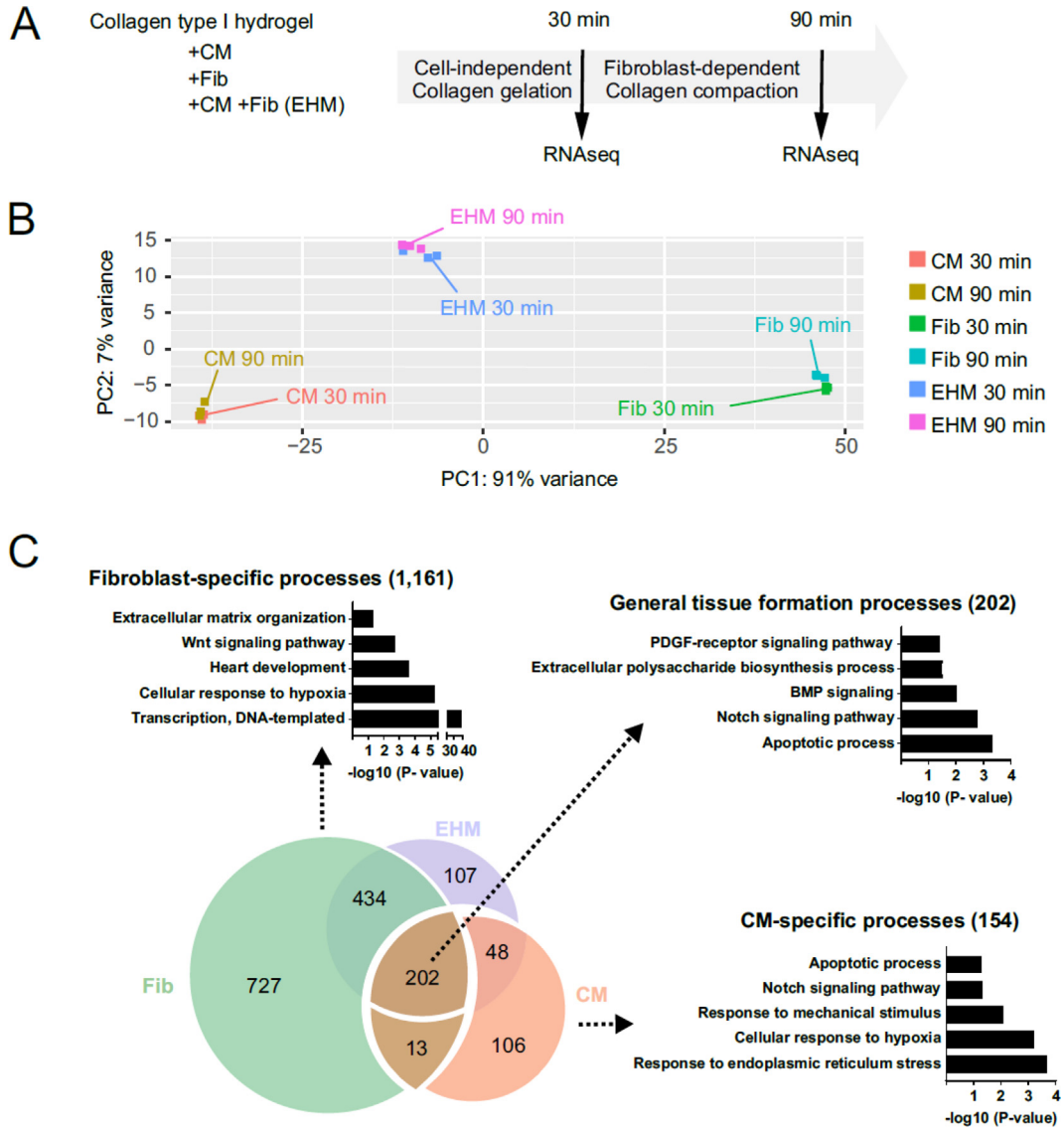

Fig. 5. Differential transcriptomes in Fibs and CM in 3D hydrogel cultures. (A) Schematic overview of the experimental design (n = 3 samples per group). (B) PCA plot of global gene expression of the respective hydrogel samples at the two investigated time-points (1: baseline after completion of cell-independent collagen gelation (30 min); 2: after additional 60 min of primarily Fib-mediated collagen compaction (90 min). (C) Venn diagram comprising the identified differentially expressed genes (DEGs) assigned to specific CM, Fib and general cell type-independent processes according to GO term analyses; all DEGs are listed in Supplementary Table 1).

especially during the early EHM formation process (Tiburcy et al., 2011). Cell loss in EHM is a combined result of irreversible damage by the enzymatic cell isolation procedure needed for EHM preparation, anoikis, and apoptosis; leading collectively to a notable change in CM:Fib composition from 2:1 (input) to 1:1 (output) during culture (Tiburcy et al., 2017). A further detailed analysis of the DEGs underlying PC2 (CM:Fib cross-talk in EHM vs the single cell culture formats) indicated 45 up- and 405 down-regulated transcripts; Supplementary Table 2), comprising a large content of non-coding RNA (210 of in total 450 transcripts, including miR and lncRNA).

2.6. Nonlinear elastic behavior at physiologically relevant strains

The rheological data reported so far were obtained at a fixed 1% strain to enable studies of the linear stress-strain response over an extended time period (60 min) under well controlled conditions (Figs. 3 and 4) without altering the collagen gelation processes. Considering that biopolymers and tissues exhibit a nonlinear strain-stiffening viscoelastic response (Storm et al., 2005) and that cardiomyocytes and cardiac muscle function at larger strains (γ_0 up to approx. 20% (Chuang et al., 2010; Hersch et al., 2013; Kajzar et al., 2008)), we performed large amplitude oscillatory shear (LAOS) measurements according to a previously reported method (Ewoldt et al., 2008) 60 min after triggering matrix consolidation by pH neutralization. LAOS allowed us to measure the stress-strain relation for one cycle as a function of time (Fig. 6A), followed by repeated measurements of the same sample at increasing strains. Plotting stress σ vs strain γ (Lissajous plot) allows for a visualization and robust quantification of the nonlinear strain-stiffening behavior (Fig. 6B). We first validated the LAOS measurements for different maximal strains ($\gamma_0 = 1\%, 2\%, 4\%, 7\%, 8\%$) on pure collagen type I networks and confirmed previous observation of strain-stiffening, which became obvious at strains $\gamma_0 > 2\%$ (Fig. 6C). We further analyzed the stress response by a Fourier analysis of the stress signal (Ewoldt et al., 2008). For reasons of symmetry, only the

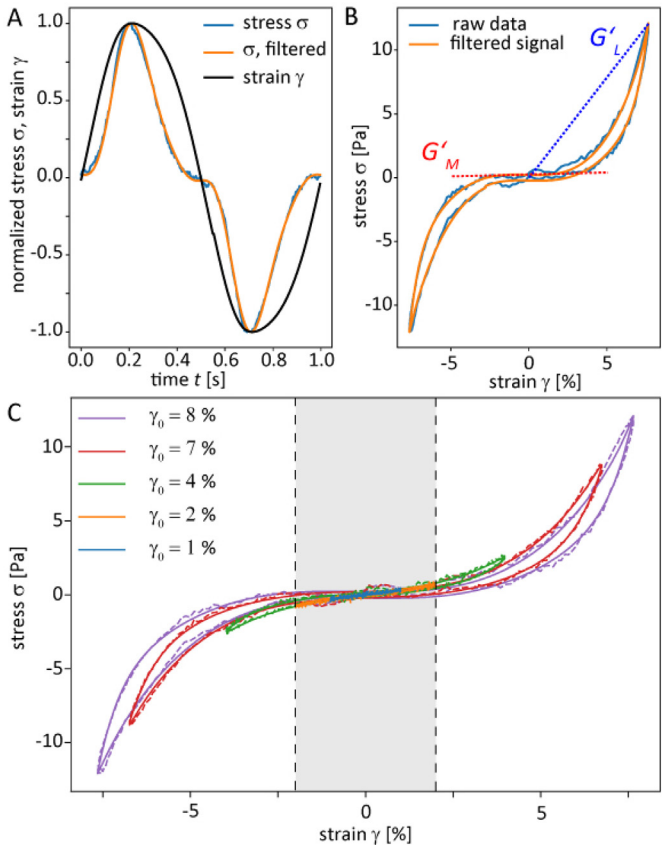

Fig. 6. Large amplitude oscillatory shear (LAOS) measurements of pH neutralized collagen hydrogels. (A) Representative data from one measurement cycle with normalized stress σ (blue) and filtered stress σ (orange) at a defined strain (γ) amplitude (black– y-axis) as a function of time (x-axis). (B) Lissajous plot transformation of the data displayed in A revealed the anticipated nonlinear stress-strain response for collagen type I networks. The raw stress signal (blue) was filtered (orange) by only using the first three non-zero, odd Fourier coefficients, i.e., the first, third and fifth Fourier mode. Indicated with dashed lines are the large-strain modulus G'_L (blue) and the minimum-strain modulus G'_M (red). (C) Lissajous plots for collagen exposed to the indicated increasing strain (γ_0) amplitudes. The raw signals are depicted as dashed lines; the filtered signals are displayed as solid lines; the different strain amplitudes are indicated by different colors. For strains $\gamma_0 = 1\%$ and 2% (range indicated in light grey between two vertical dashed lines) the measurement showed a linear relation between stress and strain, but for larger strains ($\gamma_0 > 2\%$) nonlinear strain-stiffening became evident.

first three non-zero odd Fourier coefficients, i.e., the first, third and fifth Fourier mode, were used and found sufficient to match the measured data (Fig. 6; measured stress data in blue vs. filtered stress data in orange). Therefore, the stress-strain behavior of collagen can be described in the following form:

$$\sigma(\gamma, \dot{\gamma}) = \sum_{n \in \{1,3,5\}} \left[\gamma_0 e_n T_n\left(\frac{\gamma}{\gamma_0}\right) + \gamma_0 \nu_n T_n\left(\frac{\dot{\gamma}}{\dot{\gamma}_0}\right) \right]$$

$T_n(x)$ is the n -th Chebyshev polynomial, e_n and ν_n are obtained from a Fourier transformation. Since this relation requires a strictly sinusoidal strain input, the stress response simply is a fifth-order polynomial in strain and strain rate.

In order to quantify the non-linearity of the strain response of the different samples of collagen with and without cells, we use the strain-stiffening ratio S where G'_L denotes the large-strain modulus (dashed blue line in Fig. 6B) or secant modulus at maximal strain $\gamma = \gamma_0$, G'_M (dashed red line in Fig. 6B) is the minimum-strain modulus or tangential modulus at $\gamma = 0$. A strain-stiffening ratio $S \approx 0$ indicates a linear stress-strain relation, $S > 0$ is a sign of strain stiffening (Ewoldt et al., 2008). A direct comparison of cell-free and cell-containing collagen hydrogels (Fig. 7) indicated similar strain-stiffening with however the largest S in the cell-free collagen formulation: S ($\gamma_0 = 8\%$) $= 0.849 \pm 0.017$ (collagen, n = 6), 0.710 ± 0.039 (CM, n = 3), 0.747 ± 0.027 (Fib, n = 4), and 0.675 ± 0.037 (EHM, n = 3). Collagen thus not only displays the largest stress at maximum strain ($\sigma = 8.78 \pm 0.92$ Pa), but also the most nonlinear response. Cells in general reduced strain stiffening and thus effectively softened the collagen type I hydrogels. In line with their prominent role in collagen type I hydrogel compaction (Fig. 4), Fib-populated collagen type I hydrogels exhibited a slightly higher strain-stiffening and maximal stress than CMs or CM:Fib (EHM) mixtures.

2.7. Mechanical ad-hoc model

In addition to using a Fourier analysis to obtain an expression for the stress response as a function of strain and strain rate, we established an ad-hoc model for the time dependence of the stress response that reproduces the measured stress when driven with the corresponding sinusoidal strain input. The aim was to find an expression of the form

$$\frac{d\sigma}{dt} = f(\sigma, \gamma, \dot{\gamma}; \{c_i\})$$

such that the time series $\sigma(t)$ obtained by integrating the above differential equation matches the measured stress data. $\{c_i\}$ are model parameters that can be found by minimizing the quadratic differences between the stress obtained from the model and the measured stress. The resulting model not only reproduces the measured data, but also is applicable for different than sinusoidal strain input. This is in particular important for future modelling of the more complex function of strain during a physiological contraction cycle of (engineered) human myocardium. As candidate for f we used a third order polynomial in σ, γ, and $\dot{\gamma}$. For reasons of symmetry, we considered only odd terms. During optimization we found that further terms could be omitted leaving

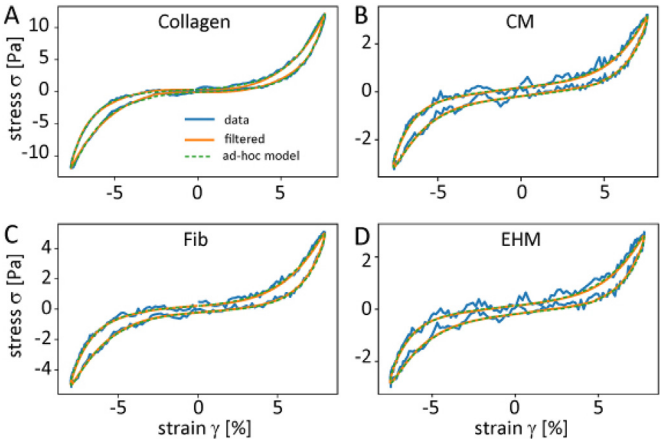

Fig. 7. Lissajous plots to assess strain-stress behavior in cell-free and cell-containing collagen type I hydrogels. All samples showed characteristic strain-stiffening. Cell-free collagen type I networks demonstrated the largest stress at maximum strain ($\sigma = 8.78 \pm 0.92$ Pa at $\gamma_0 = 8\%$; n = 6). There was a trend (not significant) towards higher strain-stiffening ($\sigma = 4.40 \pm 0.44$ Pa at $\gamma_0 = 8\%$; n = 4) by Fibs than CMs ($\sigma = 3.77 \pm 0.44$ Pa at $\gamma_0 = 8\%$; n = 3) or CM:Fib (EHM; $\sigma = 2.68 \pm 0.15$ Pa at $\gamma_0 = 8\%$; n = 3). The graphs include data from the ad-hoc model (dashed green lines) demonstrating that the observed biological phenomena can be modelled mathematically.

$$f(\sigma,\gamma,\dot{\gamma}) = c_1\gamma + c_2\dot{\gamma} + c_3\gamma^2\dot{\gamma} + c_4\gamma^2\sigma + c_5\gamma\dot{\gamma}^2 + c_6\gamma\dot{\gamma}\sigma + c_7\gamma\sigma^2 + c_8\dot{\gamma}^3 + c_9\sigma^3$$

as candidate. Optimization of the model parameters was performed using a basin-hopping algorithm (Wales and Doye, 1997). After optimization, this ad-hoc model was able to recover the measured stress data (Fig. 7). The model parameters used to obtain the curves for the four samples are listed in Supplemental Table 3.

3. Discussion

Engineering of heart muscle requires a profound understanding of cellular cross-talk and tissue biomechanics. The role of fibroblasts or fibroblast-like cells for the formation of EHM (Tiburcy et al., 2017) and similar tissue engineering approaches has been clearly recognized (Kensah et al., 2013; Naito et al., 2006; Soong et al., 2012; Zhang et al., 2013). The influence of fibroblasts on the *in vitro* heart muscle formation process becomes very obvious already within minutes to hours after EHM reconstitution, namely by its failure to compact, in the absence of fibroblasts. Here, we investigated the EHM consolidation process with a particular focus on determining the differential impact of fibroblasts and cardiomyocytes. Our data identify that the process of EHM consolidation comprises a cell-independent collagen gelation phase, followed by a fibroblast-mediated collagen compaction phase, which is likely mediated by direct fibroblast-collagen interactions via for example integrins (Herum et al., 2017). In the presence of cardiomyocytes, Fib-mediated collagen type I network compaction was clearly attenuated, suggesting a biomechanically relevant Fib:CM cross-talk. Together with the finding that environmental viscoelastic stiffening enhances extracellular matrix synthesis by Fibs and despite studying "only" engineered human heart muscle, it may be prudent to speculate that our data suggests a fibrosis control function by cardiomyocytes. The contribution of cardiomyocyte:fibroblast cross-talk to tissue fibrosis has been investigated intensively, with clear evidence for the contribution of non-coding RNA in addition to paracrine mechanisms via secreted growth factors (reviewed in (Beermann et al., 2016; Viereck et al., 2014)). The identification of a numerical model to describe the biomechanical properties, including nonlinear strain-stiffening at physiological strains, of cell-free and cell-populated collagens will not only be important for the further optimization of EHM, but may also foster our understanding of the fundamental principles underlying cell:matrix interactions for heart function in general.

We applied neonatal human foreskin fibroblasts (HFFs) rather than organ specific fibroblasts in this study for practical (homogenous, well-defined cell model) and biological reasons (similar supportive function was observed in EHM from HFF and fibroblasts of other sources, including heart; unpublished observation). Earlier data suggested that fibroblasts provide important cues for the formation of EHM, which includes the secretion and build-up of extracellular matrix (Tiburcy et al., 2011). The data obtained in this study extends our previous findings by demonstrating a transcriptional activation, which may contribute to the subsequent and continuous extracellular matrix formation processes in EHM. This appears to involve for example enhanced expression of hyaluronan synthases [HAS1 and HAS2], PDGFA, and BMP4 (common DEGs) as well as ELN (elastin), PDGFB, TGFB1, and SOX9 (Fib-specific DEGs) – all DEGs can be obtained from the Supplemental Table 1. The observed evidence for ER-stress in the cardiomyocyte pool, which may lead to the activation of apoptotic processes, is well in line with the observed enhanced caspase activity during the early EHM formation process (Tiburcy et al., 2011). Several means have been developed to counter cardiomyocytes loss in EHM, including the application of cardio-protective molecules such as insulin/IGF-1 (Naito et al., 2006) and PDGF-BB (Vantler et al., 2010). The obtained evidence of non-coding RNA mediated cross-talk between fibroblasts and cardiomyocytes in EHM (Supplemental Table 2) was a notable observation and will require further detailed studies, including studies on exosome/microvesicle mediated cross-talk, a mechanisms described to in tumor environment stiffening (Bonnans et al., 2014; Villasante et al., 2016), and analyses of proteome alterations by the observed non-coding RNA as well as the associated consequences for the long-term regulation of ECM viscoelasticity.

A particular goal of this study was to go beyond the description of biological processes and potentially involved mechanisms and establish the basis for the formulation of mechanical models of the EHM formation process. For this, viscoelastic properties of collagen type I and its alterations in the presence of the key cellular components of EHM, i.e., cardiomyocytes and fibroblasts, must be provided. By *in situ* rheological measurements we collected quantitative data of G′ and G″ during early cell-independent and cell/Fib-dependent tissue compaction as well as important insight into the nonlinear strain stiffening properties of collagen without or populated with cells. An interesting observation was the cell-induced softening of collagen at high strains. This may be explained by the soft mechanical properties of cells per se and is in line with studies on the biomechanics of multi-component tissues (Huber et al., 2013; Marquez et al., 2010). Activation of cell intrinsic and mainly fibroblast-associated mechanisms appears to counter the softening process, likely by additional extracellular matrix synthesis and mechanical pre-straining of the extracellular matrix into the nonlinear strain-stiffening range. In essence, fibroblasts and cardiomyocytes in collagen type I hydrogels appear to self-organize the EHM formation process by a dynamic adaptation of the viscoelastic properties of the surrounding extracellular matrix environment. Finally, the introduced numerical ad-hoc model is a first step towards future simulations of the viscoelastic properties of EHM (Stein et al., 2017), in particular with respect to the more complex stress-strain relation during a contraction cycle. In combination with novel models of cross-linked and anisotropic networks (Heidemann et al., 2015, 2018) this may allow for the identification of ideal cell compositions and externally imposed stress-strain behavior, either by mechanical means (Liaw and Zimmermann, 2016) or electrical stimulation (Godier-Furnemont et al., 2015) for optimal tissue development.

4. Materials and methods

4.1. Cell culture

Human neonatal foreskin fibroblasts (Fibs) were obtained from ATCC (HFF-1, SCRC-1041) and maintained in DMEM containing 4 mM L-glutamine, 4,500 mg/L glucose, 1 mM sodium pyruvate, and 1,500 mg/L sodium bicarbonate supplemented with 15% fetal calf serum (FCS), 100 U/mL Penicillin, and 100 μg/mL Streptomycin (P/S; Thermo Scientific). Cell counting was done with a CASY TTC system (Roche) using the electric current exclusion method. Fibs were used for experiments from passage 18–22. Cardiomyocytes were derived from HES2 (ES International, Singapore) or a genetically modified derivative HES2-RFP (Irion et al., 2007). Ethical approval for the use of human embryonic stem cells (ESCs) was obtained from the Central Ethic Committee for Stem cell Research (ZES; permit #12; reference number: 1710-79-1-4-16). ESCs were grown and differentiated as reported previously (Tiburcy et al., 2017). Cardiomyocyte purity was analyzed by flow cytometry (Fig. 1B).

4.2. Flow cytometry

Single cardiomyocyte cell suspensions were prepared by digesting cardiomyocyte monolayers with a mixture of Accutase (Millipore), 0.0125% Trypsin (Thermo Scientific), and 20 μg/ml DNAse (Calbiochem) for 15–30 min at room temperature. Fibroblasts were prepared by digestion with TrypLE (Thermo Sientific) for 10 min at 37 °C. Cells were resuspended in culture medium, centrifuged at 300 g for 5 min, and incubated with 1:1,000 Sytox Red Dead Cell Stain (5 μmol/L stock solution; Thermo Scientific) and Brilliant Stain Buffer containing mouse anti-human BUV395-conjugated CD90 IgG1,κ (BD Biosciences, clone 5E10, 5 μl per sample) for 20 min at 4 °C. CM suspensions were centrifuged at 300 g for 5 min and then fixed in 70% ice-cold ethanol. After fixation, cells were centrifuged once more and resuspended in blocking buffer (PBS containing 1 mg/ml BSA [Sigma], 5% FCS [Thermo Fisher] and 0.1% Triton 100X [Sigma]). After 10 min of blocking, cells were pelleted by centrifugation and resuspended in blocking buffer with primary antibody (sarcomeric α-actinin 1:4,000 Sigma-Aldrich A7811, mouse-monoclonal) or respective IgG1 isotype control for 45 min at 4 °C. Cells were washed twice with PBS, followed by a washing step in blocking buffer and subsequent incubation in secondary antibody (1:1,000 anti-mouse 488 [A-11001] or 633 [A-21052], Thermo Fisher) and Hoechst (10 ng/ml; Thermo Fisher) for 30 min at 4 °C. Cells were washed with PBS and finally resuspended in PBS for analysis. The gating strategy was described in detail in (Tiburcy et al., 2017). 10,000 live cell events were analyzed per sample. Measurements were performed on a LSRII SORP Cytometer and analyzed using the DIVA software (BD Biosciences). FACS visual plots were generated using Flowing Software 2.5.1. (Perttu Terho, University of Turku, Finland).

4.3. Hydrogel culture preparations and analysis

Two batches of medical-grade bovine collagen (LLC Collagen Solutions) were used in this study (Batch 1:15CSA02; Batch 2: 17CSA03). Equal volumes of collagen (0.9 mg/ml) and concentrated serum-free medium (2x RPMI, 8% B27 without insulin, 200 U/ml penicillin, and 200 μg/ml streptomycin) were mixed on ice. Cells (950,000 Fibs/ml, 1,900,000 CMs/ml, or both cell types at a 1:2 ratio - 2,850,000 cells/ml) were added after pH neutralization by dropwise addition of 0.1 N NaOH. Single cell suspensions were prepared as described above for the flow cytometry experiments. Cells were suspended in EHM culture medium: Iscove's medium with 4% B27 without insulin, 1% non-essential amino acids, 2 mmol/l glutamine, 300 μmol/l ascorbic acid, 100 ng/ml IGF1 (AF-100-11), 10 ng/ml FGF-2 (AF-100-18B), 5 ng/ml $VEGF_{165}$ (AF-100-20), 5 ng/ml TGF-β1 (AF-100-21C), and P/S (all growth factors were obtained from PeproTech). An equal amount of EHM culture medium without cells was added in the cell free, collagen only, conditions. 149 and 450 μl hydrogel:cell mixtures were used for to rheology measurements or cast into circular models to generate tissue loops (Soong et al., 2012; Tiburcy et al., 2017). Hydrogel consolidation was studied for 60 min in a bulk rheometer or after 24 and 72 h in the circular casting molds. The size of compacted hydrogels and total arm thickness of 4-week-old tissues was determined using a Lumar system equipped with an AxioCam MRc and Axiovert 4.1 software (Zeiss). For the latter analyses 10–20 individual measurements of tissue thickness per tissue were averaged.

4.4. Histology

For whole-mount analyses, hydrogels/EHM were fixed in 4% formaldehyde (Histofix, Roth) for at least 2 h at room temperature. After washing for 4 h at room temperature (RT) in blocking buffer (PBS containing 1 mg/ml bovine serum albumin [Sigma], 5% FCS [Gibco], and 0.1% Triton [Sigma]) the primary antibodies were added for 48 h at 4 °C. Following three washes with PBS for 60 min at RT the secondary antibodies, together with phalloidin (Thermo Scientific), were added for 48 h at 4 °C. After three more washes, tissues were mounted with Fluoromount (SouthernBiotech) and imaged using a Zeiss confocal microscope (CLSM; Zeiss 710 LSM/NLO). For cryo-sectioning, tissues were immersed in 30% sucrose overnight at 4 °C and embedded the following day in OCT (TissueTech) by slow freezing on a liquid nitrogen-cooled metal block. Tissues were stored at −20 °C and cut at 10 μm with a cryotome (Leica). Tissues were dried at RT before blocking for 30 min and treated with primary antibodies (or respective isotype controls) overnight at 4 °C, followed by three washes with PBS for 20 min and incubation with secondary antibody and Hoechst for 2 h at RT. After three final washes, tissue mounting was with Fluoromount (SouthernBiotech). Sections were imaged using a Zeiss confocal microscope (CLSM; Zeiss 710 LSM/NLO). For Sirius Red staining, tissues were embedded in paraffin (Roth). 4 μm sections were cut, dewaxed, and rehydrated using standard protocols. Nuclei were stained with Mayer's Hemalaun solution (AppliChem) for 5 min. After two washes with H_2O slides were incubated with Picrosirius red solution for at least 1 h. Subsequently, the slides were washed twice with acetic acid (5% v/v in H_2O) for 5 min, followed by clearing in xylol (Roth). Slides were mounted using Histokitt II (Roti). Slides were imaged using a Zeiss Axiovert microscope and analyzed using ZEN software.

4.5. Contraction analysis

Tissue constructed in a loop format, were isometrically suspended in organ baths (Föhr Medical Instruments) filled with Tyrode's solution (in mmol/L: 120 NaCl, 1 MgCl2, 0.2 CaCl2, 5.4 KCl, 22.6 NaHCO3, 4.2 NaH2PO4, 5.6 glucose, and 0.56 ascorbate) at 37 °C and constant bubbling with 5% CO_2 and 95% O_2. Force of contraction measurements were performed at 1.5 Hz electrical field stimulation with 5 ms square pulses (200 mA) and calcium concentrations increasing from 0.2 to 4 mmol/L as described previously (Tiburcy et al., 2017).

4.6. Rheometry

Mechanical properties of the hydrogel samples with and without cells were investigated with a bulk rheometer (MCR-501, Anton Paar, Austria) using a cone and plate geometry with an angle of 2° and a gap height of 103 μm. The temporal evolution of the mechanical properties were monitored with measurements every 30 s using a sinusoidal strain of 1% at 1 Hz. This low strain ensures to be in the linear response regime and does not alter the gelation process (data not shown). Dehydration of the sample was avoided by keeping the environment in a custom-made measurement chamber saturated with water vapor. The temperature was kept constant at 23 °C. For the nonlinear analysis the built-in LAOS routines of the rheometer software were used. The general setup was the same as described above and LAOS measurements were performed directly after finishing the measurement of the temporal evolution (on the same sample). While the frequency of the strain input remained at 1 Hz the strain amplitude was increased from $\gamma_0 = 1\%$ to $\gamma_0 = 10\%$ in steps of 1%. The stress response over one period of oscillation (i.e. 1 s) was recorded and stress data were sampled with 256 points per period (every 3.9 ms).

4.7. RNAseq

To simulate the conditions used for the rheology measurements,

cell:collagen mixtures were incubated at 23 °C for 30 and 90 min before snap freezing the reconstitution mixtures in liquid nitrogen and extracting RNA using the TRIZOL method (Thermo Scientific). Quality and integrity of RNA was assessed with the Fragment Analyzer from Advanced Analytical by using the standard sensitivity RNA Analysis Kit (DNF-471). RNA-seq libraries were prepared using a modified strand-specific, massively-parallel cDNA sequencing (RNA-Seq) protocol from Illumina, the TruSeq Stranded Total RNA (Cat.No. RS-122-2301). Libraries were sequenced on a HiSeq 4000 platform (Illumina) generating 50 bp single-end reads (30–40 Mio reads/sample). Sequence images were transformed with Illumina software BaseCaller to BCL files, which was demultiplexed to fastq files with bcl2fastq v2.17.1.14. The quality check was done using FastQC (version0.11.5, BabrahamBioinformatics). Sequence reads were aligned to the human genome reference assembly (UCSC version hg19) using Bowtie 2.0 (Langmead and Salzberg, 2012). For each gene, the number of mapped reads was counted using HTSeq-counts; and DESeq2 was used to analyze the differential expression (Anders and Huber, 2010). DEGs were identified by a log2-fold difference of 0.5 in transcript levels between the 30 min and 90 min time-points according to the Benjamini-Hochberg method for multiple comparisons (adjusted $P < 0.05$). Gene ontology (GO) analyses were performed using DAVID (Huang da et al., 2009a; Huang da et al., 2009b). VennDiagrams were generated using BioVenn (Hulsen et al., 2008).

4.8. Statistical analysis

Data are displayed as mean ± standard error of the mean (SEM). Figure captions include information about the applied statistical test methods and sample sizes. Statistical significance was assumed when $p < 0.05$. Statistical test were performed using GraphPad software (version 7).

Acknowledgements

This work was funded via the Collaborative Research Center SFB 937, projects A13 (F.R.) and A18 (S.L., U.P., W.H.Z.). M.T. and W.H.Z. receive additional support from SFB 1002 C04 and S01, IRTG 1816 RP12, and DZHK. We acknowledge the excellent technical assistance of Andreas Schraut, Iris Quentin, Krasimira Sharkova, Daria Reher and Monika Hoch in the generation of HES2-derived CMs, routine culture of Fibs, and Sirius red staining of slides. We are grateful to Elina Grishina for immunostaining of EHM time-series cryosections. The support by Gabriela Salinas, Orr Shomroni and the technical staff of the Transcriptome and Genome Analysis Laboratory (TAL) at the University Medical Center Göttingen is greatly acknowledged.

Appendix A. Supplementary data

Supplementary data to this article can be found online at https://doi.org/10.1016/j.pbiomolbio.2018.11.011.

References

Anders, S., Huber, W., 2010. Differential expression analysis for sequence count data. Genome Biol. 11, R106.
Beermann, J., Piccoli, M.T., Viereck, J., Thum, T., 2016. Non-coding RNAs in development and disease: background, mechanisms, and therapeutic approaches. Physiol. Rev. 96, 1297–1325.
Bonnans, C., Chou, J., Werb, Z., 2014. Remodelling the extracellular matrix in development and disease. Nat. Rev. Mol. Cell Biol. 15, 786–801.
Chuang, J.S., Zemljic-Harpf, A., Ross, R.S., Frank, L.R., McCulloch, A.D., Omens, J.H., 2010. Determination of three-dimensional ventricular strain distributions in gene-targeted mice using tagged MRI. Magn. Reson. Med. 64, 1281–1288.
Ewoldt, R.H., Hosoi, A.E., McKinley, G.H., 2008. New measures for characterizing nonlinear viscoelasticity in large amplitude oscillatory shear. J. Rheol. 52, 1427–1458.
Gao, L., Gregorich, Z.R., Zhu, W., Mattapally, S., Oduk, Y., Lou, X., Kannappan, R., Borovjagin, A.V., Walcott, G.P., Pollard, A.E., Fast, V.G., Hu, X., Lloyd, S.G., Ge, Y., Zhang, J., 2018. Large cardiac muscle patches engineered from human induced-pluripotent stem cell-derived cardiac cells improve recovery from myocardial infarction in swine. Circulation 137, 1712–1730.
Godier-Furnemont, A.F., Tiburcy, M., Wagner, E., Dewenter, M., Lammle, S., El-Armouche, A., Lehnart, S.E., Vunjak-Novakovic, G., Zimmermann, W.H., 2015. Physiologic force-frequency response in engineered heart muscle by electromechanical stimulation. Biomaterials 60, 82–91.
Godier-Furnémont, A.F.G., Tiburcy, M., Wagner, E., Dewenter, M., Lämmle, S., El-Armouche, A., Lehnart, S.E., Vunjak-Novakovic, G., Zimmermann, W.-H., 2015. Physiologic force-frequency response in engineered heart muscle by electromechanical stimulation. Biomaterials 60, 82–91.
Hanley, K.P., Oakley, F., Sugden, S., Wilson, D.I., Mann, D.A., Hanley, N.A., 2008. Ectopic SOX9 mediates extracellular matrix deposition characteristic of organ fibrosis. J. Biol. Chem. 283, 14063–14071.
Heidemann, K.M., Sageman-Furnas, A.O., Sharma, A., Rehfeldt, F., Schmidt, C.F., Wardetzky, M., 2018. Topology counts: force distributions in circular spring networks. Phys. Rev. Lett. 120, 068001.
Heidemann, K.M., Sharma, A., Rehfeldt, F., Schmidt, C.F., Wardetzky, M., 2015. Elasticity of 3D networks with rigid filaments and compliant crosslinks. Soft Matter 11, 343–354.
Hersch, N., Wolters, B., Dreissen, G., Springer, R., Kirchgeßner, N., Merkel, R., Hoffmann, B., 2013 Mar 15. The constant beat: cardiomyocytes adapt their forces by equal contraction upon environmental stiffening. Biol. Open 2 (3), 351–361. https://doi.org/10.1242/bio.20133830.
Herum, K.M., Lunde, I.G., McCulloch, A.D., Christensen, G., 2017. The soft- and hard-heartedness of cardiac fibroblasts: mechanotransduction signaling pathways in fibrosis of the heart. J. Clin. Med. 6.
Huang da, W., Sherman, B.T., Lempicki, R.A., 2009a. Bioinformatics enrichment tools: paths toward the comprehensive functional analysis of large gene lists. Nucleic Acids Res. 37, 1–13.
Huang da, W., Sherman, B.T., Lempicki, R.A., 2009b. Systematic and integrative analysis of large gene lists using DAVID bioinformatics resources. Nat. Protoc. 4, 44–57.
Huber, F., Schnauß, J., Rönicke, S., Rauch, P., Müller, K., Fütterer, C., Käs, J., 2013. Emergent complexity of the cytoskeleton: from single filaments to tissue. Adv. Phys. 62, 1–112.
Hulsen, T., de Vlieg, J., Alkema, W., 2008. BioVenn – a web application for the comparison and visualization of biological lists using area-proportional Venn diagrams. BMC Genomics 9, 488.
Irion, S., Luche, H., Gadue, P., Fehling, H.J., Kennedy, M., Keller, G., 2007. Identification and targeting of the ROSA26 locus in human embryonic stem cells. Nat. Biotechnol. 25, 1477.
Kajzar, A., Cesa, C.M., Kirchgeßner, N., Hoffmann, B., Merkel, R., 2008. Toward physiological conditions for cell analyses: forces of heart muscle cells suspended between elastic micropillars. Biophys. J. 94, 1854–1866.
Kensah, G., Roa Lara, A., Dahlmann, J., Zweigerdt, R., Schwanke, K., Hegermann, J., Skvorc, D., Gawol, A., Azizian, A., Wagner, S., Maier, L.S., Krause, A., Dräger, G., Ochs, M., Haverich, A., Gruh, I., Martin, U., 2013. Murine and human pluripotent stem cell-derived cardiac bodies form contractile myocardial tissue in vitro. Eur. Heart J. 34, 1134–1146.
Lacraz, G.P.A., Junker, J.P., Gladka, M.M., Molenaar, B., Scholman, K.T., Vigil-Garcia, M., Versteeg, D., de Ruiter, H., Vermunt, M.W., Creyghton, M.P., Huibers, M.M.H., de Jonge, N., van Oudenaarden, A., van Rooij, E., 2017. Tomo-seq identifies SOX9 as a key regulator of cardiac fibrosis during ischemic injury. Circulation 136, 1396–1409.
Langmead, B., Salzberg, S.L., 2012. Fast gapped-read alignment with Bowtie 2. Nat. Methods 9, 357.
Li, Y., Lui, K.O., Zhou, B., 2018. Reassessing endothelial-to-mesenchymal transition in cardiovascular diseases. Nat. Rev. Cardiol.
Liaw, N.Y., Zimmermann, W.H., 2016. Mechanical stimulation in the engineering of heart muscle. Adv. Drug Deliv. Rev. 96, 156–160.
Marquez, J.P., Elson, E.L., Genin, G.M., 2010. Whole cell mechanics of contractile fibroblasts: relations between effective cellular and extracellular matrix moduli. Phil. Trans. Math. Phys. Eng. Sci. 368, 635–654.
Naito, H., Melnychenko, I., Didié, M., Schneiderbanger, K., Schubert, P., Rosenkranz, S., Eschenhagen, T., Zimmermann, W.-H., 2006. Optimizing engineered heart tissue for therapeutic applications as surrogate heart muscle. Circulation 114. I-72-I-78.
Ronaldson-Bouchard, K., Ma, S.P., Yeager, K., Chen, T., Song, L., Sirabella, D., Morikawa, K., Teles, D., Yazawa, M., Vunjak-Novakovic, G., 2018. Advanced maturation of human cardiac tissue grown from pluripotent stem cells. Nature 556, 239–243.
Soong, P.L., Tiburcy, M., Zimmermann, W.H., 2012. Cardiac differentiation of human embryonic stem cells and their assembly into engineered heart muscle. Current Protocols Cell Biol. 55, 23.28.1-23.8.21.
Stein, S., Luther, S., Parlitz, U., 2017. Impact of viscoelastic coupling on the synchronization of symmetric and asymmetric self-sustained oscillators. New J. Phys. 19, 063040.
Storm, C., Pastore, J.J., MacKintosh, F.C., Lubensky, T.C., Janmey, P.A., 2005. Nonlinear elasticity in biological gels. Nature 435, 191–194.
Tiburcy, M., Didie, M., Boy, O., Christalla, P., Doker, S., Naito, H., Karikkineth, B.C., El-

Armouche, A., Grimm, M., Nose, M., Eschenhagen, T., Zieseniss, A., Katschinksi, D.M., Hamdani, N., Linke, W.A., Yin, X., Mayr, M., Zimmermann, W.H., 2011. Terminal differentiation, advanced organotypic maturation, and modeling of hypertrophic growth in engineered heart tissue. Circ. Res. 109, 1105–1114.

Tiburcy, M., Hudson, J.E., Balfanz, P., Schlick, S., Meyer, T., Chang Liao, M.-L., Levent, E., Raad, F., Zeidler, S., Wingender, E., Riegler, J., Wang, M., Gold, J.D., Kehat, I., Wettwer, E., Ravens, U., Dierickx, P., van Laake, L.W., Goumans, M.J., Khadjeh, S., Toischer, K., Hasenfuss, G., Couture, L.A., Unger, A., Linke, W.A., Araki, T., Neel, B., Keller, G., Gepstein, L., Wu, J.C., Zimmermann, W.-H., 2017. Defined engineered human myocardium with advanced maturation for applications in heart failure modeling and repair. Circulation 135, 1832–1847.

Tiburcy, M., Meyer, T., Soong, P.L., Zimmermann, W.H., 2014. Collagen-based engineered heart muscle. Methods Mol. Biol. 1181, 167–176.

Vantler, M., Karikkineth, B.C., Naito, H., Tiburcy, M., Didié, M., Nose, M., Rosenkranz, S., Zimmermann, W.-H., 2010. PDGF-BB protects cardiomyocytes from apoptosis and improves contractile function of engineered heart tissue. J. Mol. Cell. Cardiol. 48, 1316–1323.

Viereck, J., Bang, C., Foinquinos, A., Thum, T., 2014. Regulatory RNAs and paracrine networks in the heart. Cardiovasc. Res. 102, 290–301.

Villasante, A., Marturano-Kruik, A., Ambati, S.R., Liu, Z., Godier-Furnemont, A., Parsa, H., Lee, B.W., Moore, M.A., Vunjak-Novakovic, G., 2016. Recapitulating the size and cargo of tumor exosomes in a tissue-engineered model. Theranostics 6, 1119–1130.

Wales, D.J., Doye, J.P.K., 1997. Global optimization by basin-hopping and the lowest energy structures of Lennard-Jones clusters containing up to 110 atoms. J. Phys. Chem. 101, 5111–5116.

Weinberger, F., Breckwoldt, K., Pecha, S., Kelly, A., Geertz, B., Starbatty, J., Yorgan, T., Cheng, K.H., Lessmann, K., Stolen, T., Scherrer-Crosbie, M., Smith, G., Reichenspurner, H., Hansen, A., Eschenhagen, T., 2016. Cardiac repair in Guinea pigs with human engineered heart tissue from induced pluripotent stem cells. Sci. Transl. Med. 8, 363ra148.

Zhang, D., Shadrin, I.Y., Lam, J., Xian, H.-Q., Snodgrass, H.R., Bursac, N., 2013. Tissue-engineered cardiac patch for advanced functional maturation of human ESC-derived cardiomyocytes. Biomaterials 34, 5813–5820.